

# The Coaxial High Energy Thruster

IEPC-2005-100

Presented at the 29<sup>th</sup> International Electric Propulsion Conference, Princeton University,  
October 31 – November 4, 2005

Flavio Poehlmann\*, Nicolas Gascon†, Cliff Thomas‡, Mark Cappelli§  
Stanford University, Stanford, CA 94305, USA

## Abstract

This paper describes our efforts on the development of a high power pulsed coaxial plasma accelerator. The particular discharge configuration is a revisit of a concept that was originally proposed in 1970 [D.Y. Cheng, Nuclear Fusion **10**, “*Plasma Deflagration and the Properties of a Coaxial Plasma Deflagration Gun*”, 1970]. From previous studies, high reported exhaust velocities of up to  $3 \times 10^6$  m/s, and thrust densities on the order of  $10^5$  N/m<sup>2</sup> make this Coaxial High ENerGy Thruster (CHENG Thruster) very attractive for a variety of space missions. However, the plasma acceleration mechanism is not well understood and the high power requirements of several kilojoules per pulse in the early designs may pose some practical limitations for near-term applications. Therefore, a scaled down version of a CHENG thruster has been designed and will be used to characterize the plasma and electromagnetic properties in the near-field and in the thruster discharge chamber. This paper reintroduces the concept of the thruster, presents an overview of the known physics, and describes the scaled thruster design and preliminary characterization of the pulsed propellant valve.

## Nomenclature

$\vec{A}$	= magnetic potential vector
B	= azimuthal magnetic field
$\vec{B}$	= magnetic field vector
C	= electromagnetic Chapman-Jouguet speed
$c_{\text{sound}}$	= speed of sound
$\vec{E}$	= electric field vector
e	= internal energy
H	= Hugoniot constant
h	= enthalpy
I	= total current
J	= current density
L	= energy lost
l	= characteristic length scale of thruster
m	= mass of the particle
$m_i$	= ion mass
p	= pressure
$p^*$	= total pressure

---

\* Research Assistant, Mechanical Engineering, flaviop@stanford.edu

† Research Associate, Mechanical Engineering, nicolas.gascon@stanford.edu

‡ Research Assistant, Mechanical Engineering, saber@stanford.edu

§ Professor, Mechanical Engineering, cap@stanford.edu

$Q$	= energy input
$q_e$	= elementary charge
$R$	= gas constant
$R_A$	= anode radius
$r_L$	= Larmor radius
$T$	= apparent temperature
$T^*$	= total temperature
$t$	= time
$V$	= volume
$\vec{v}$	= velocity vector
$\vec{x}$	= location vector
$Z$	= number of charges on each ion
$\gamma$	= specific heat ratio
$\epsilon$	= electric permittivity
$\mu$	= magnetic permeability
$\mu_0$	= permeability constant
$v_A$	= Alfvén velocity
$\rho$	= density
$\phi$	= applied potential

## I. Introduction

This paper describes our initial efforts on the development of a high power, high density, pulsed coaxial plasma accelerator referred to here as a “Coaxial High ENerGy (CHENG) Thruster”. The concept of this thruster and most of the existing theoretical and experimental knowledge originated from the discharge studies of Cheng [1], at the University of Santa Clara starting in the late 1960s. Although this device was initially designed as a plasma injector for nuclear fusion experiments, its characteristics make the CHENG thruster attractive for orbit raising and interplanetary travel, especially for missions to the outer planets and beyond. In these early experiments this thruster processed peak input powers on the order of gigawatts to yield super-Alfvén exhaust velocities of up to  $3 \times 10^6$  m/s at a thrust density of  $10^5$  N/m<sup>2</sup>. The particle number density inside the thruster was on the order of  $10^{15}$  cm<sup>-3</sup> and typical pulse durations lasted approximately 10  $\mu$ s. The high specific impulse and thrust density was reportedly accompanied by low electrode erosion, probably due to a thick (diffuse) discharge region, and also by low beam divergence. While research efforts on the thruster started more than four decades ago, the plasma acceleration mechanism is still not well understood. This is attributed to the very limited theoretical, experimental, and numerical models of the thruster, as much of the early work was under restricted distribution following its initial discovery. Compared to other high  $I_{sp}$  thrusters, such as the magnetoplasmadynamic (MPD) thruster, the CHENG thruster offers significantly lower erosion rates and even higher exhaust velocities. However, the high peak power requirements necessitate high capacity energy storage systems which may impose significant mass penalties.

Figure 1 shows a schematic illustration of one of Cheng’s original coaxial discharge cavities [1]. This version was operated with a 12 KJ capacitor bank and a voltage of approximately 20 kV across the electrodes. The capacitors are initially connected to the electrodes and when charged,

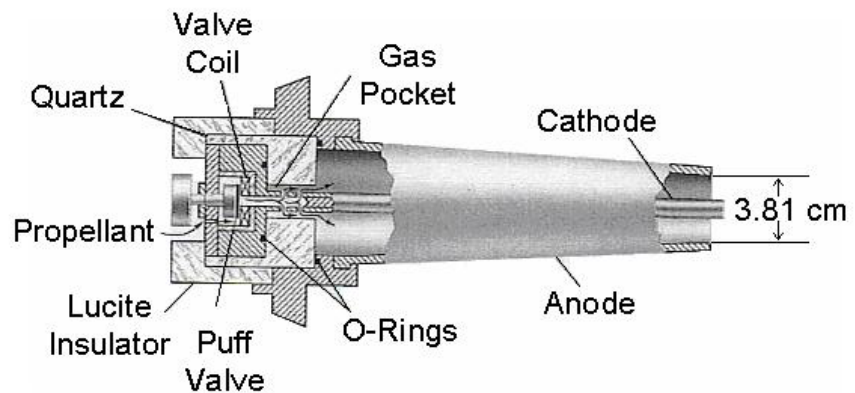


**Figure 1:** Schematic of a 12 KJ co-axial high energy discharge [1].

electrical breakdown is held off on the vacuum side of the Paschen curve. The discharge is then initiated by a puff of gas, such as hydrogen or xenon, injected at the breach of the thruster through a fast acting valve which opens and closes on the order of a few microseconds. Upon entering the co-axial channel, the gas immediately breaks down. This is followed by rapid avalanche ionization, and the resulting current induces an azimuthal magnetic field. The electromagnetic force then accelerates the ions to very high exhaust velocities. A particular advantage of this mode of operation is that the valve acts as the switch that initiates and terminates the discharge pulse. Therefore, the control circuitry is relatively simple and efficient propellant utilization is expected.

Stanford's present activities focus on developing a better understanding of the physics governing thruster operation and scaling. The present high power requirements and associated mass of the capacitor bank may pose practical limitations for near-term space propulsion applications. A better understanding of the governing physics should make it possible to build smaller thrusters that operate at lower total thrust levels and lower voltages, while still achieving comparatively high specific impulse and thrust densities. Therefore, we have designed a scaled down version of a CHENG thruster, which operates at an estimated 3 kJ per pulse. This version is intended for use in the laboratory to characterize the plasma and electromagnetic field inside the thruster, and to validate the scaling laws.

This paper is organized as follows: In the next section, we review Cheng's early theoretical work [1, 2]. This is followed in Section III by a discussion of numerical simulations, including a review of simulations carried out at Stanford that date back to 1969 [3], and also preliminary simulations carried out by us using a commercially available Particle-In-Cell code (OOPIC Pro [4]). In Section IV, we describe the scaling of Cheng's original thruster and some practical challenges associated with implementing this thruster as a realistic option for space propulsion. In Section V we discuss the design of our 3 kJ thruster, and preliminary characterization of the pulsed valve operation. We conclude by outlining future work.

## II. The Deflagration Analogy

The only theoretical description of this co-axial discharge that is published in the open literature is that presented by Cheng [1]. It is well known that one-dimensional compressible flow of a magnetized plasma of infinite conductivity gives rise to the magnetohydrodynamic analogue of the Rankine-Hugoniot equation [5], which is commonly used in gas dynamics to describe the jump conditions across a shock wave. When heat is released to the flow (non-adiabatic flow) this equation describes the solutions to the mass, momentum and energy equations applied across a one-dimensional combustion wave. Such a case can be generated in the laboratory as a wave traveling in a tube that is filled with a premixed combustible gas mixture. If the reference frame is attached to the wave, then the reactants enter the combustion region (i.e., approach the combustion wave) with velocity  $u_1$ , pressure  $p_1$ , internal energy  $e_1$ , and density  $\rho_1$ . The products then leave the combustion region with velocity  $u_2$ , pressure  $p_2$ , internal energy  $e_2$ , and density  $\rho_2$ . The process releases a given amount of chemical energy  $Q = e_2 - e_1$ . The Hugoniot curve, schematically illustrated in Fig. 2, describes the combinations of  $p_2$  and  $1/\rho_2$  that satisfy the three conservation laws. These solutions are divided into regions by drawing tangents to the curve through the origin A ( $p_1, 1/\rho_1$ ) which describes some initial state, and vertical and horizontal lines from A describing constant density and constant pressure transitions, respectively. The Chapman-Jouguet (C-J) points U and L in Fig. 2 mark the solutions at which the combustion wave travels at sonic speeds. Regions I and II correspond to strong and weak detonation and regions III and IV to weak and strong deflagration, respectively. According to Cheng [1], the high exhaust velocities and low erosion rates of the CHENG thruster can be explained by introducing the concept of a "plasma deflagration". A short overview of the Rankine-Hugoniot concept in chemical combustion is given next, before it is applied to an electric discharge. As a full discussion of the Rankine-Hugoniot curve for chemical combustion is beyond the scope of this paper, the interested reader is referred to the book by Kuo [6].

Figure 2 shows that a detonation causes both pressure and density to increase across the combustion wave. In practice, such a situation can be observed by closing the tube on one end and igniting the gas mixture at the closed end. The combustion wave then travels down the tube in the form of a

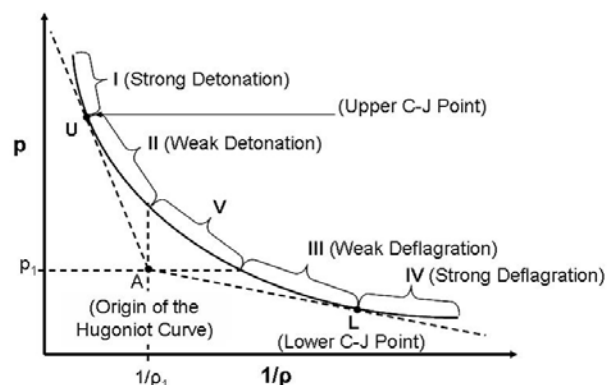


Figure 2: Hugoniot curve.

shock and compresses the gas in front of it. In this case, the products of combustion and the shock itself move in the same direction. At solution U, the combustion wave travels at sonic speed whereas it is supersonic for regions I and II. In the reference frame of the detonation wave, a strong detonation decelerates the gas from supersonic to subsonic speed, whereas a weak detonation decelerates the particles to a lesser extent so that they remain supersonic. Region V in Figure 2 is physically impossible as it would require imaginary particle velocities in order to satisfy the conservation laws.

A deflagration can be achieved by igniting the combustible gas mixture at the open end of the tube. The combustion wave then travels into the tube and the burned gas is accelerated outwards. Since the burned gas and the combustion wave now travel in opposite directions, a deflagration causes both the pressure and the density to drop across the combustion wave. Therefore, a deflagration wave does not compress and heat the gas to the same extent as a detonation. As a result, combustion in a deflagration mode has a significant advantage over detonation. It converts more of the released chemical energy into directed kinetic energy rather than random thermal energy. Thus deflagration is more efficient at accelerating a gas. The C-J point L in Fig. 2 corresponds to the solution at which the deflagration wave travels at sonic speed. This is the maximum wave speed possible in the deflagration mode and the wave speed is subsonic for solution regions III and IV. In the reference frame of the combustion wave, a weak deflagration accelerates the unburned gas from a subsonic to a higher subsonic speed. A strong deflagration, on the other hand, accelerates particles from subsonic to supersonic speeds. From a propulsion point of view, a strong deflagration is thus an attractive solution as it could yield very high exhaust velocities. But from the second law of thermodynamics and from wave structure considerations it follows that not all solutions of the Hugoniot curve are accessible, and solutions U and III are the ones most commonly observed in experiments. Therefore, chemical rockets operate in a weak deflagration mode and accelerate the subsonic burned gas to supersonic velocities using a De Laval nozzle.

It is noteworthy that most magnetohydrodynamic treatments of shock waves in plasmas deal with adiabatic flow (see for example, Sutton and Sherman [5]), where the deflagration branch is not accessible because of second law considerations. This restriction is lifted for non-adiabatic flow in the case of combustion waves [7]. It is argued by Cheng [1] that the performance of the CHENG thruster is the result of a strong plasma deflagration, made possible by the rapid Joule heating of the gas in a discharge zone, analogous to the rapid chemical heat release in the reaction zone of a combustion wave. Deflagration waves are known to be relatively thick, the characteristics of which are determined by mass and energy diffusion [6], and such a diffuse plasma deflagration can account for the low electrode erosion seen in these coaxial guns [1]. If indeed a strong plasma deflagration is accessible in the CHENG thruster, it is shown below that it is possible to reach super-Alfvén exhaust velocities without the usual magnetic nozzle. A strong deflagration is believed to be the cause for the high particle velocities ( $3 \times 10^6$  m/s) observed in these early experiments.

Figure 3 depicts a one-dimensional model of an electric discharge in a duct. The coordinate system is chosen such that it makes the wave, in this case the high current region, stationary. Zone 1 contains the unprocessed neutral gas and zone 2 consists of a thin collisionally dominated ionization front followed by a thick heating and expansion region. This expansion region ends when the velocity of the plasma in the  $\mathbf{J} \times \mathbf{B}$  direction is higher than the thermal velocity of the charged particles. Zone 3 then corresponds to a region of collisionless acceleration. If it is assumed that all the energy is added to the plasma in zone 2, the mass, momentum and energy conservation laws can be applied across zone 2, taking into consideration the states of the propellant within zones 1 and 3. However, for the case of a plasma, the conservation equations also have to account for the magnetic pressure  $B^2/2\mu_0$  and the work required to fill the specific volume with magnetic field  $B^2/2\rho\mu_0$ . The modified mass, momentum and energy equations then become:

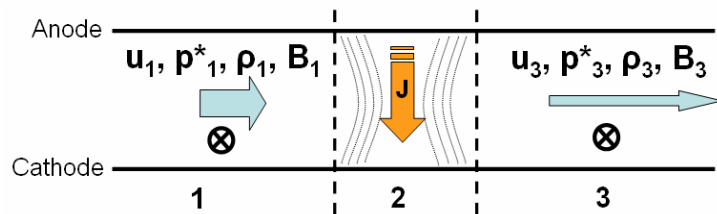


Figure 3: One-dimensional model of a plasma deflagration.

$$\rho_1 u_1 = \rho_3 u_3 \quad (1)$$

$$\rho_1 u_1^2 + p_1 + \frac{B_1^2}{2\mu_0} = \rho_3 u_3^2 + p_3 + \frac{B_3^2}{2\mu_0} \quad (2)$$

$$h_1 + \frac{1}{2}u_1^2 + \frac{B_1^2}{2\rho_1\mu_0} + q = h_3 + \frac{1}{2}u_3^2 + \frac{B_3^2}{2\rho_3\mu_0} + L \quad (3)$$

Introducing the modified pressure,  $p^*$  and temperature  $T^*$ :

$$p^* = \left( p + \frac{B^2}{2\mu_0} \right) = \rho RT^* \quad (4)$$

Equations (1), (2) and (3) can be combined to eliminate the velocity terms  $u_1$  and  $u_2$ . After some algebra an expression is obtained that resembles the Rankine-Hugoniot relationship:

$$H = Q - L = e_3 - e_1 + \frac{1}{2} \left( \frac{1}{\rho_3} - \frac{1}{\rho_1} \right) (p_3^* + p_1^*) \quad (5)$$

The only difference to the familiar Hugoniot relationship from combustion theory is that the pressures  $p_1$  and  $p_3$  have been replaced with  $p_1^*$  and  $p_3^*$  to incorporate the magnetic fluid contributions. By letting  $e = c_v T$  and  $\gamma = c_p/c_v$ , it can be shown [1] that the speed of the wave,  $C$ , at the C-J points, is slightly smaller than the Alfvén velocity

$$v_A = \sqrt{\frac{B_1^2}{\rho_1\mu_0}}, \text{ i.e.,}$$

$$C^2 = \gamma \left( \frac{p}{\rho} + \frac{B^2}{2\rho\mu_0} \right)_1 = c_{\text{sound}}^2 + \frac{\gamma}{2} v_A^2 \quad (6)$$

Assuming a magnetic field of 1 Tesla and a hydrogen number density of  $1 \times 10^{15} \text{ cm}^{-3}$ , the Alfvén velocity  $v_A$  is approximately  $7 \times 10^5 \text{ m/s}$ . Under the right conditions, the discharge wave can be made stationary at the breach of the thruster and if a strong plasma deflagration could be achieved, the particles leaving the discharge zone would need to have velocities larger than  $C$ . Since the reported exhaust velocities of up to  $3 \times 10^6 \text{ m/s}$  are about four times larger than  $v_A$  and at the same time do not exceed it by more than an order of magnitude, it seems possible that the CHENG thruster is operating in a strong deflagration mode.

### III. Results from Simulation

The most extensive numerical study of this co-axial deflagration thruster was performed by Watson in 1969 [3]. Watson argues that the main difference in the accelerating mechanism between the MPD arcjet and the thruster of Cheng [1] is the importance of particle collisions within the accelerator. This difference is illustrated in Fig. 4. In the MPD thruster, the charged particle path lengths are long enough so that the charged particles are deflected between collisions by the magnetic field and receive a component of velocity in the  $\mathbf{J} \times \mathbf{B}$  direction. Most of the electrical energy is given to the electrons and since collisions are sufficiently frequent, the electrons transfer their directed energy to the ions by collisions (Fig. 4a). For the case of the CHENG thruster, the charged particle path lengths are significantly longer, and as a result the electrons cannot transfer a significant amount of energy to the ions. Instead, the ions receive most of their energy directly from the electric field and as they accelerate, they are increasingly deflected in the axial direction by the azimuthal magnetic field. Eventually the forces due to the radial electric field and the azimuthal magnetic field cancel and the ion leaves the thruster moving in the axial direction (Fig. 4b).

Watson argues that for particle velocities of  $10^5 \text{ m/s}$  or larger and for number densities of  $10^{15} \text{ cm}^{-3}$  or smaller, a collisionless plasma model is applicable and there exists a “free-fall region” inside the CHENG thruster for which these conditions exist. But while collisions may not be a primary mechanism for accelerating the plasma, they are necessary for producing the plasma. Watson resolves this apparent contradiction by assuming a high density region between the point of gas injection and the upstream edge of the free fall region. Arguing that the gas velocity near the point of entry should be on the order of the thermal velocity of  $10^4 \text{ m/s}$ , he arrives at the conclusion that the number density near the gun breach is two orders of magnitude higher than in the remaining parts of the thruster. The collisionality thus is high enough in that region to provide a sufficient amount of ionization. Watson considers this region as a source of the plasma and simulates only the downstream collisionless regime of direct

electromagnetic acceleration. In addition, he assumes that the plasma is fully ionized and hence he ignores neutrals in his simulation. For his calculations, he uses discretized approximations to the exact equations of motion:

$$d\vec{v} = Z \frac{q_e}{m} (\vec{E} + \vec{v} \times \vec{B}) dt \quad (7)$$

$$d\vec{x} = \vec{v} dt \quad (8)$$

as well as the usual field equations:

$$\vec{E} = -\nabla\phi - d\vec{A}/dt \quad (9)$$

$$\vec{B} = \nabla \times \vec{A} \quad (10)$$

where the electric and magnetic potentials are defined as:

$$\phi = \int_{\text{allspace}} \frac{\rho}{4\pi\epsilon R} dV \quad (11)$$

$$\vec{A} = \int_{\text{allspace}} \frac{\mu J}{4\pi R} dV \quad (12)$$

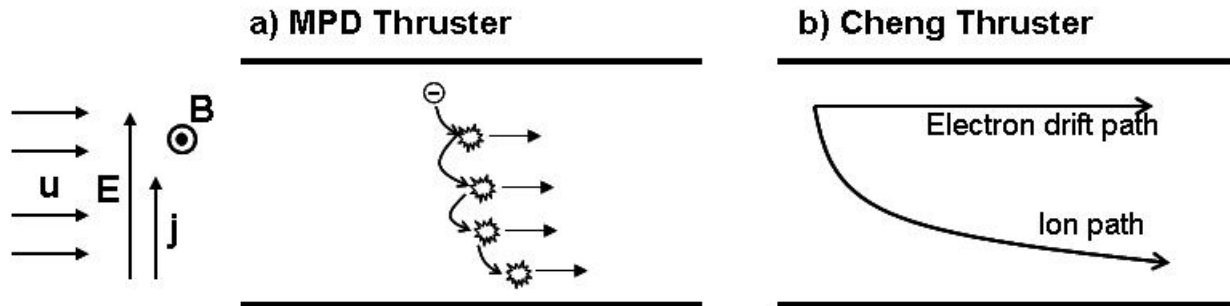


**Figure 4:** (a) Transfer of magnetic body force to gas stream by electron collisions [8], (b) electron and ion trajectories in a uniform electric field and a magnetic field that decays in the axial direction [3].

When particles collide with the thruster walls, he assumes that they are reflected specularly but return with half their kinetic energy. The exception on this condition is that electrons hitting the anode are absorbed and ions hitting the cathode are neutralized. The values of exhaust velocities, thrust and voltage calculated from his simulations agree with the experimental data reported by Cheng [1] within the accuracy of the measurements. In addition, his simulations yield some further interesting results. (i) Due to the absence of collisions, the  $\rho_i \mathbf{E}$  force is not cancelled by the  $\rho_e \mathbf{E}$  force and becomes the dominant force term for imparting energy to the ions. Initially, the  $\rho_i \mathbf{E}$  force on a newly born ion only has to overcome the inertia force. However, towards the end of the ion trajectory, the  $\rho_i \mathbf{E}$  force is balanced by the  $\mathbf{v}_i \times \mathbf{B}$  force of the magnetic field, and the ion moves in the axial direction. (ii) The self-induced magnetic field causes a large fraction of the electrons emitted from the cathode to be deflected from their radial trajectory to an axial path. Most of the electrons emitted from the cathode leave the thruster forming the neutral plasma exhaust stream. The electron current is mainly supplied by electrons released by ionization of the gas. The increase in electron density near the axis lowers the electric potential along the axis such that it becomes mainly radial. This provides the potential drop to accelerate the ions which are then deflected in the axial direction by the self-induced magnetic field. In addition, it was found that approximately half of the total radial current can be attributed to the ions. (iii) The simulations suggest that the propellant mass flow for optimum operation and the specific impulse are proportional to the total current. The voltage and thrust, on the other hand, scale with the square of the current. Finally, perhaps most important from a scaling viewpoint, the simulations also suggest similitude in accordance with the following non-dimensional parameters:

$$\left(\frac{Ze}{m_i}\right)\phi\left(\frac{\Delta t}{l}\right)^2, \quad \mu\left(\frac{Ze}{m_i}\right)I\left(\frac{\Delta t}{l}\right), \quad \mu\left(\frac{Ze}{m_i}\right)^2\dot{m}\left(\frac{\Delta t}{l}\right)$$

In other words, a given simulation applies to any combination of applied voltages, currents, mass flow rates, accelerator sizes, and time scales that have the same dimensionless parameters indicated above.

#### IV. Discussion of the Theoretical and Numerical Models

If the theory as proposed by Watson [3] is correct, it implies that the maximum ion gyro radius has to be approximately equal to the size of the thruster and to the size of the volume that contains a large magnetic field. This seems to be the case as the reported exhaust velocities of  $10^6$  m/s and a magnetic field on the order of 1 Tesla correspond to an ion Larmor radius of 1 cm, which matches the characteristic length scale of the thruster.

Furthermore, in the absence of collisions and other large loss or accelerating mechanisms, the final velocity of the ions should be consistent with the potential energy difference of the electric field through which the ion has fallen. For the case of the 20kV thruster operated by Cheng this would correspond to a maximum exhaust velocity of approximately  $2 \times 10^6$  m/s, which agrees well with Cheng's measurements [1].

In addition, the assumption of collisionless acceleration needs to be further examined. Watson states that the ion-ion energy exchange cross section is  $10^{-20}$  cm<sup>2</sup> for particles moving at  $10^6$  m/s. At a number density of  $10^{15}$  cm<sup>-3</sup> this corresponds to a mean free path between ion-ion collisions on the order of 1 km. Since the energy exchange cross-section for electron-ion collisions should be even smaller, it appears that the assumption of collisionless acceleration is satisfied. However, it has to be kept in mind that particles accelerate to this speed, and furthermore, while the absolute speed of ions may reach  $10^6$  m/s, the relative speed between ions moving in the same direction may be significantly lower and thus their cross sections may appear larger in a moving reference frame. Therefore, the mean free path is likely to be much shorter than 1 km, perhaps as low as 1 m. This is still long compared to the characteristic thruster dimensions, which are on the order of centimeters, and the collisionless assumption still seems plausible.

It is also interesting to calculate the mean free path for the ionization of neutral hydrogen atoms and check if it is consistent with the model in Ref. [3]. The ionization cross section reported is  $10^{-17}$  cm<sup>2</sup> or larger. This corresponds to an average ionization path length of 1cm in the high density ionization region and of 1 m in the free fall region. Thus the assumption that the high density region may serve as a plasma source for the downstream free fall region seems reasonable.

While it seems that the simulated thrust and exhaust velocities of Watson [3] agree with the estimates of Cheng [1], the question remains in how far this model is consistent with the low erosion rates observed. It seems reasonable that the collisionless free fall region simulated causes little erosion on the electrodes. From the typical ion trajectory illustrated in Fig. 4b and in the absence of collisions it can be seen that those ions having fallen through a significant portion of the electric potential have also been deflected the most by the magnetic field. So the fastest moving ions either hit the cathode with a small radial velocity component or not at all. The ions that do hit the cathode with a considerable radial velocity component are most likely the ones that were born close to the cathode. The damage imparted by these ions is less severe because the ions did not have the chance to fall through a significant portion of the electric field to achieve high velocities.

Some consideration must be given to the structure of the thin high density region upstream of the free fall region where most of the ionization takes place. As mentioned earlier, the number density in that region may be two orders of magnitude higher than downstream of the deflagration wave and the collisionality in this region could be high enough to

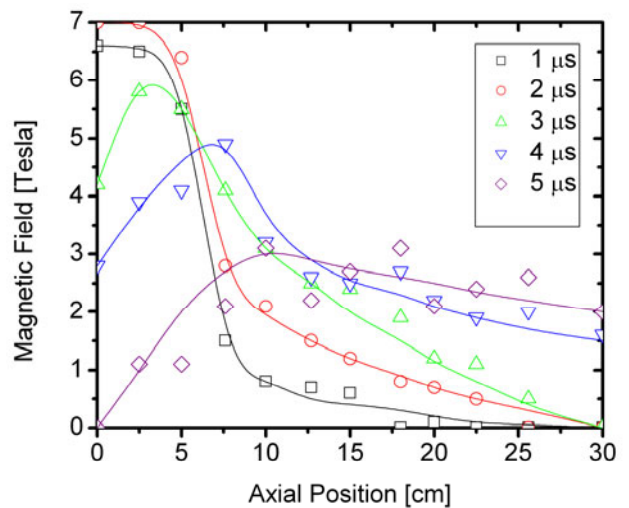


**Figure 5:** Magnetic field profile inside thruster cavity as a function of time during deflagration discharge [1].

cause a high current density on the electrodes. However, a closer examination reveals that this is probably not the case due to strong confinement of the charged particles. As can be seen from the experimental data in Fig. 5, the magnetic field measured by Cheng [1] during the first three microseconds of the pulse is strongest near the breach of the thruster and is approximately an order of magnitude higher than in the collisionless direct electromagnetic acceleration region further downstream. Therefore, the magnetic deflection of the ions in the ionization region is also stronger. This in turn allows the ions to only fall through a smaller fraction of the potential field and thus they gain less speed. As a result of these two combined effects the ion Larmor radius is reduced by several orders of magnitude and becomes small compared to the thruster dimensions and the mean free path. The ion Hall parameter, therefore, is much larger than unity despite the increased collisionality in the ionization region and thus the ions mainly drift downstream without imparting significant damage to the cathode.

This conjecture was tested in preliminary simulations performed using the commercially available PIC code OOPIC Pro [4]. Due to the difficulties associated with applying a commercial program to a problem as specific as this, some compromising assumptions had to be made. For example, the current version of OOPIC Pro is not able to compute the self-induced magnetic field in the simulation. So, instead, the experimentally-measured magnetic field profile after 2  $\mu\text{s}$  [1], as shown in Fig. 5, was applied to the simulation. In addition, the simulation was performed ignoring collisions and assuming full ionization. As seen from the computed axial ion velocity shown in Fig. 6 (for the 12 kJ thruster case [1]), the results are in good agreement with the measured ion velocities at the thruster exit, and show that the ions and electrons are indeed very strongly confined near the breach of the thruster and slowly drift downstream. When the particles reach the axial position characterized by the strong negative gradient in magnetic field, the Larmor radius increases, the ions are allowed to drop through a bigger portion of the electric field and thus rapidly accelerate. The ions are accelerated until the condition of direct electromagnetic acceleration is achieved [1, 3]. These results suggest that the strong gradient in magnetic pressure plays a significant role in the operation of the thruster.

The results from the simulation show some consistencies with the deflagration model description. The magnetic pressure and the density decrease across the deflagration wave, the accelerated particles move in the opposite direction as the ionization wave and the ionization wave is moving towards the higher pressure region. Similar to the chemical combustion case, the energy added to the flow goes directly into accelerating the gas, instead of compressing and heating it as would be the case for a detonation. In addition, the negative gradient in magnetic pressure is essential to ensure operation in the deflagration mode. This condition is equivalent to the aforementioned example of igniting a premixed combustible gas mixture from the open end of the tube.

However, these observations do not answer the question of why it is believed that a strong deflagration is possible in a plasma whereas it is never seen in a combustion wave. It should be pointed out that the results from the simulations do fit the characteristics of a strong deflagration as described in Fig. 2. The speed of the ionization front determined by the simulation and also from measurements by Cheng [1] is very low and at times even stationary. This suggests that the thruster may be operating either near the intersection of regions III and V of Fig. 2 or at a point very far to the right on the  $1/\rho$  axis. But the first case would correspond to a very small change in pressure and density which clearly is not the case. Instead, a significant pressure and density gradient is observed which suggests that the thruster is operating in region IV, i.e. in a strong deflagration mode. Unlike combustion waves, with heat transport driven by the release of the limited chemical potential energy, this electrical discharge results in a much larger heat addition than usually seen in a combustion wave. We believe that this unusual supply of thermal energy and differences in wave structure result in the transition from a weak to a strong deflagration. However, this is still to be verified.

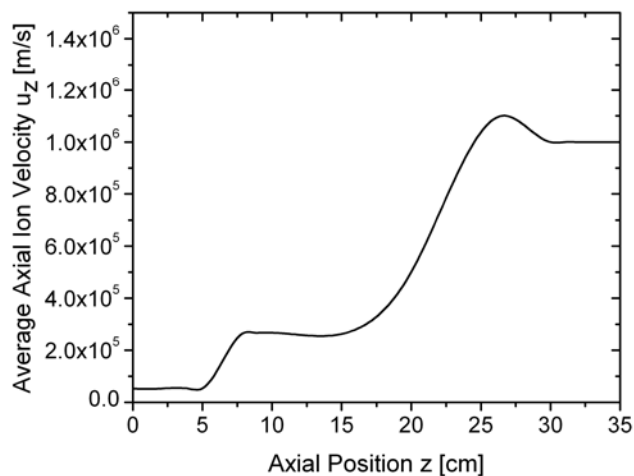


**Figure 6:** Average axial ion velocity versus axial location from OOPIC Pro simulation of Cheng's 12 kJ thruster.

## V. Current and Planned Activities at Stanford University

The high thrust density, low beam divergence and low erosion rates make the CHENG thruster very attractive for a variety of space propulsion applications. The first three columns of Table 1 compare the performance of a Hall thruster, a typical MPD thruster and the 12 kJ CHENG thruster for a spacecraft that has 1 kW of electrical power available for propulsion. It can be seen that the time-averaged thrust of the CHENG thruster is 15 times lower than for the MPDT and 30 times lower than for the Hall thruster. However, the total impulse per propellant mass consumed is approximately 25 times higher than for the MPDT and 170 times higher than for a Hall thruster. This shows that a CHENG thruster, in its original form, would have to be operated on a long mission, for example, to the outer planets, to outperform the Hall thruster or MPDT. Like the MPDT, which is also more suited for deep space missions, the CHENG thruster faces the additional challenge of requiring energy storage for pulsed operation. However, the CHENG thruster reportedly lacks the severe electrode erosion problems that currently limit MPDT applications.

**Table 1:** Relative performance at 1 kW available steady state power: Hall thruster, 3 MW MPDT (quasi-steady pulsed), 1 GW CHENG thruster (quasi-steady pulsed), and scaled CHENG thruster.

	Hall Thruster	MPD Thruster	CHENG Thruster [1]	Scaled CHENG Thruster
Avg. Propellant Mass Flow	$4 \times 10^{-3}$ g/s	$3 \times 10^{-4}$ g/s	$8 \times 10^{-7}$ g/s	$8 \times 10^{-5}$ g/s
Pulse Frequency	Continuous	1 Hz	0.08 Hz	83 Hz
Time Averaged Thrust	0.06 N	0.03 N	0.002 N	0.02 N
Impulse / Propellant Mass	15 Ns/g	100 Ns/g	2,500 Ns/g	250 Ns/g

Motivated by these findings, Stanford is reintroducing the CHENG thruster with the intention of exploring scaled down versions for near-term space application. Examples for such applications are orbit raising and missions to the outer and inner planets. According to Watson, the collisionless model employed in these early simulations is applicable to plasma accelerators that operate at specific impulses of  $10^4$ s or more. Taking  $10^4$ s as a lower limit and using the scaling relations determined in Ref. [3], a preliminary analysis suggests that the CHENG thruster could be scaled down to operate at 200V with the performance characteristics shown in column 4 of Table 1. Depending on the desired combination of pulse frequency and length, the scaled thruster would require relatively small capacitors. If the quasi-steady pulse duration is kept at 10 $\mu$ s the pulse frequency could be increased to 83 Hz. This would reduce the requirements on capacitor storage capability to 12 J instead of the 12kJ used in the early versions. The time averaged thrust would be about 24 mN - within 40% of the thrust of a 1 kW Hall thruster. At the same time the propellant mass utilization of the CHENG thruster could still be an order of magnitude higher than that of the Hall thruster.

If the early experimental results [1, 2] can be reproduced and if the scaling relations of Ref. [3] are confirmed, the CHENG thruster may offer alternatives for a wide variety of applications, ranging from orbit transfer to deep space travel. In addition, such a thruster is well suited for taking advantage of the higher power that may be provided by future space qualified nuclear reactors. The CHENG thruster could provide the high thrust levels required for manned interplanetary missions without suffering from the erosion problems of other high  $I_{sp}$  devices.

For our preliminary experimental studies, we have designed a CHENG thruster that operates at 3 kJ per pulse. Figure 7 shows the Stanford CHENG thruster mounted to a fast-acting beam valve for propellant injection. The length of the anode tube is 10.2 inches and its inner diameter is 1.9 inches. The outer diameter of the cathode is 0.25 inches. The anode disc, cathode disc and valve are separated from each other by 0.75 inch thick acrylic insulators.

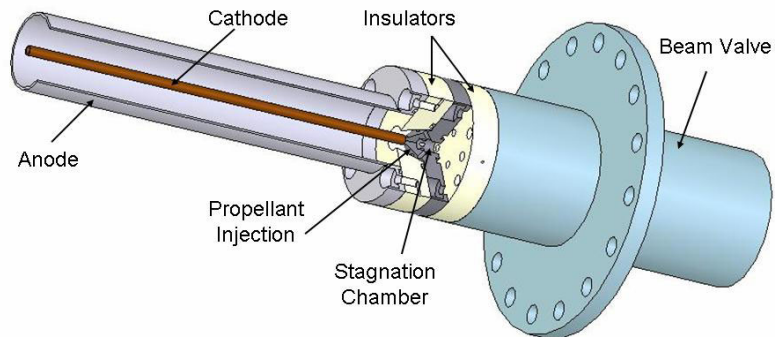


**Figure 7:** The Stanford 3 kJ CHENG Thruster.

The valve injects the propellant into a 0.2 inch diameter channel that traverses the insulator and terminates in a small chamber at the cathode base. The propellant stagnates in the chamber and then enters the thruster cavity through sixteen 1/8 inch diameter holes in the chamber walls. This design ensures that the propellant enters the electrode gap with a uniform front. The following few paragraphs explain how the dimensions were determined for this thruster.

The scaled thruster was designed to have the same ratio of ion Larmor radius  $r_L$  to anode radius  $R_A$  as Cheng's original thruster [1] but to operate with a quarter of the power. For a given propellant type, the ratio  $r_L/R_A$  scales with the square root of the applied voltage and inversely with the magnetic field  $B$  and radius  $R_A$ .  $B$ , however, scales with the current  $I$  and inversely with  $R_A$ . If these two relations are combined to eliminate  $B$ ,  $R_A$  cancels and it is found that the applied voltage has to scale with the square of the current. This is the same result as Watson had achieved in his simulations. In order to operate at a quarter of the power, the applied voltage of the scaled thruster thus has to be reduced from 20,000 to approximately 8,000 V.

Furthermore, the scaled thruster should have a similar ratio of total current to propellant mass flow as in the early thrusters [3], and the number density should be approximately the same for both. Therefore, the mass flow rate is proportional to  $R_A^2$ . From this it follows that the anode radius of the scaled thruster should be half as large as that of Cheng's 12kJ thruster.

A crucial component for the operation of the thruster is the propellant valve. It has to be able to deliver a peak mass flow rate on the order of 1 g/s over a timeframe of just a few microseconds. These requirements are met by the Jordan C-211 Pulsed Beam Valve. This valve employs the magnetic beam repulsion principle illustrated in Fig. 8. If a high current is passed through the beam conductor, the generated magnetic force causes the top beam to be lifted from the O-ring seal over the nozzle, allowing gas to flow through it.

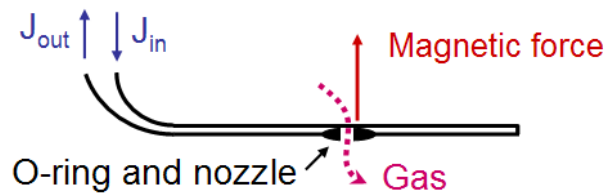


**Figure 8:** Magnetic beam repulsion principle used in the fast pulsed beam valve.

The user can apply a back pressure of up to 10 atm and use nozzles with diameters between 0.1 and 1 millimeter. Therefore, mass flow rates on the order of 1 g/s and lower can be achieved. Depending on the amount of current that is passed through the beam conductors, the pulse width of the gas should be around 20  $\mu$ s. The pulse width can be measured using a fast ionization gauge. In a preliminary experiment, the beam valve was used to inject air through a 0.5 mm nozzle at a back pressure of 1 atm. Figure 9 shows the reading of the fast ionization gauge. Since the gauge was not installed right in front of the nozzle, but on the opposite wall of the chamber and offset from the valve axis, the signal is distorted by reflections of the particles off the chamber walls. In addition, using a gas mixture (air) instead of a uniform gas caused further distortion of the signal. Ideally, one would hope for a near trapezoidal shape of the signal. Nevertheless, the preliminary results show that the gas puff caused a pressure spike that lasted approximately 20  $\mu$ s.

Once completed, the scaled version of this thruster is intended for use in the laboratory to characterize the plasma and electromagnetic field inside the discharge cavity. Modern diagnostics will be used to first reproduce past experimental results and then to expand the experimental database. In addition, long time operation will be tested to verify and quantify the reported low electrode erosion rates. In parallel to the experimental efforts, numerical work is being performed to better understand the accelerating mechanism and correlate to experimental data. Due to the better computing resources available today, these simulations will be able to incorporate higher levels of complexity, such as modeling neutrals and ionization. As more physical insight is gained on the accelerating mechanism, the next step will be to continue the scaling process and study smaller thrusters.

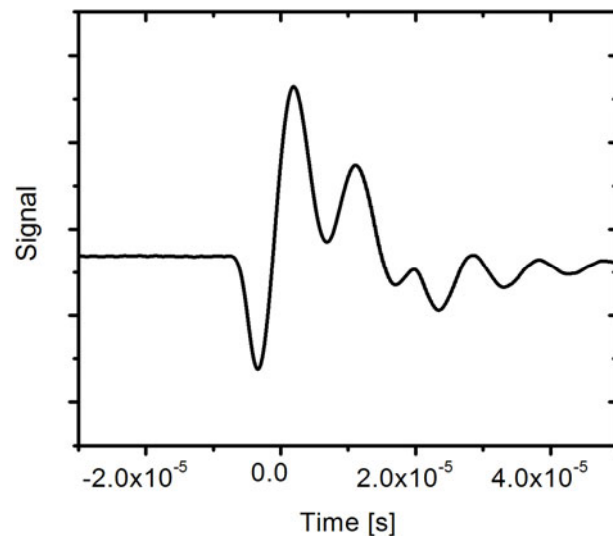


**Figure 9:** Fast ionization gauge signal of gas puff injected into vacuum chamber using a fast pulsed beam valve.

## VI. Conclusions

This paper reintroduced the concept of a Coaxial High ENerGy (CHENG) plasma accelerator, which had been initially studied in the 1960s, and provided an overview of the present state of knowledge based on the available literature. In its original form the CHENG thruster processed powers on the order of Gigawatts and produced ion exhaust velocities on the order of  $10^6$ m/s at a thrust density of  $10^5$ N/m<sup>2</sup>. A theoretical model based on one-dimensional non-adiabatic flow was described suggesting that the acceleration process is similar to that of a strong plasma deflagration. Past numerical simulations were reviewed, and the resulting scaling relations were discussed. It appears that the mass flow and specific impulse scale with the current and that the required voltage and thrust scale with the square of the current. These scaling laws can be used to design lower power thrusters, which can serve as propulsion sources, in applications that are currently dominated by ion and Hall thrusters. Should higher power levels become available in space, the CHENG thruster is suited to provide the high thrust levels needed for manned interplanetary travel without the serious electrode erosion problems of other high power thrusters that compete for these applications, such as MPDTs. A 3kJ CHENG source has been designed and is currently being assembled that will be used to characterize the plasma and electromagnetic field inside the thruster. Finally, we have initiated a numerical study based on Particle-In-Cell (PIC) simulations to better understand the plasma acceleration mechanism.

## Acknowledgements

The authors would like to extend their appreciation to Prof. D.Y. Cheng, for the many stimulating discussions, the donation of valuable equipment, and for introducing us to this interesting propulsion concept. We would also like to acknowledge Dr. Jean-Luc Cambier (AFRL) for providing the needed power supplies and access to the OOPIC code, and Dr. William Hargus (AFRL) for some fabricated thruster components. Finally, we would like to thank Paul Shoessow, John Cary and Peter Stoltz at Tech-Ex, for guidance in carrying out the OOPIC simulations, and our colleague Ms. Emmanuelle Sommier for assistance in the fabrication of the Stanford thruster.

## References

- [1] Cheng, D.Y., “*Plasma Deflagration and the Properties of a Coaxial Plasma Deflagration Gun*”, Nuclear Fusion 10, 1970
- [2] Cheng, D.Y., “*Application of a Deflagration Plasma Gun as a Space Propulsion Thruster*”, AIAA Journal Vol.9, No.9, September 1971
- [3] Watson, V.R., “*Computer Simulation of a Plasma Accelerator*”, Ph.D. Dissertation, Stanford University, 1969
- [4] OOPIC Pro Version 1.0 Research, Tech-X Corporation, Boulder, CO
- [5] Sutton, G.W., Sherman, A., “*Engineering Magnetohydrodynamics*”, McGraw-Hill, 1965
- [6] Kuo, K.K., “*Principles of Combustion*”, John Wiley and Sons, 1986
- [7] Oosthuizen, P.H., Carscallen, W.E., “*Compressible Fluid Flow*”, McGraw-Hill, 1997
- [8] Jahn, R.G., “*Physics of Electric Propulsion*”, McGraw-Hill, 1968